

MRI: a possible mechanism for funnel flows?

S. Doğan^{1,2} and E. R. Pekünlü¹

¹*Department of Astronomy and Space Sciences, Faculty of Science, University of Ege, 35100, Bornova, İzmir, Turkey*

²*Theoretical Astrophysics Group, University of Leicester, Leicester LE1 7RH, UK*

suzan.dogan@ege.edu.tr

ABSTRACT

The magnetorotational instability (MRI) has been suggested to have an important role on the dynamics of accretion disks. We investigate MRI as an alternative way for guiding the plasma from the disk to the funnel flow at the disk-magnetosphere boundary of classical T Tauri stars (CTTSs) by considering the diamagnetic effects. We solve the magnetohydrodynamic equations by including the effect of both the magnetic field gradient and the perpendicular (to the field) velocity gradient produced by the magnetization current at the disk-magnetosphere boundary for the first time. *Diamagnetic current modified MRI* produces a non-propagating mode which may lift the plasma from the disk towards the vertical magnetic field lines. Our model also shows that the diamagnetic effects play an important role in triggering the MRI. The instability becomes more powerful with the inclusion of the gradient in the magnetic field and the perpendicular velocity.

Subject headings: Accretion, accretion disks – instabilities – MHD – plasmas

1. Introduction

One of the unsolved problems related to the accretion of matter onto a rotating star with a dipole magnetic field is identifying the mechanism that guides the plasma from the disk into the funnel flow (FF) (see Ghosh & Lamb 1978; Pringle & Rees 1972; Romanova et al. 2002). The basic picture of the disk-magnetosphere interaction in magnetized stars is generally described as follows: It is commonly assumed that the accretion flow is disrupted within the magnetospheric boundary layer where the magnetic forces become dominant in determining the motion of the plasma, then the plasma is funneled onto the polar caps of the star. However, the interaction between the disk and the magnetosphere is exceedingly complicated.

Over the last few decades, there have been a number of theoretical efforts to understand the nature of the disk-magnetosphere interaction in a magnetized star (e.g. Pringle & Rees 1972; Lamb et al. 1973; Ghosh & Lamb 1978; Camenzind 1990; Königl 1991; Spruit & Taam 1993; Shu et al. 1994; Lovelace et al. 1995; Li et al. 1996.). The magnetospheric accretion models were proposed first for neutron stars and

black holes. Then, these models were adopted and developed for magnetic T Tauri stars. Johns-Krull & Gafford (2002) examined three analytic theories assuming that accretion is controlled by magnetosphere in classical T Tauri stars (CTTSs). They claim that while the surface magnetic fields of BP Tau and TW Hya are not dipolar, it is likely that the dipole component dominates at the inner disk-magnetosphere boundary. They suggest that the disk truncation radii in CTTSs is in the stellar radius range of $3R_*$ - $6R_*$, where the dipole component governs the disk-magnetospheric interaction. Küker, Henning & Rüdiger (2003) also studied the disk dipolar magnetic field interaction in CTTSs. They found the critical field strength for the disk disruption to lie between 1 and 10 kG. They also consider the possibility of the drainage at the inner parts of the disk by magnetically enhanced accretion.

In recent years, several authors presented observational evidences for the magnetospheric funnels on to CTTSs. Muzerolle et al. (1998) used the model favouring magnetospheric accretion through dipole magnetic field lines and successfully explained the observed spectral line shapes. Stempels & Piskunov (2002) presented the results of observations done with UVES/VLT on one of the CTTSs RU Lup. Their main interest was to reveal the properties and geometry of the accretion process. The authors reported that the observational results were in agreement with the magnetospheric accretion model. Stempels & Piskunov (2002) argue that magnetic accretion model proved itself to be consistent with some of the emission lines' radiative transfer calculations. Magnetospheric accretion model for neutron stars introduced by Ghosh & Lamb (1979) later applied to T Tauri stars by Uchida & Shibata (1985) and Königl (1991) is regarded as consistent with complex observational picture in CTTSs case by Stempels & Piskunov (2002). By using Doppler imaging technique, Strassmeier et al. (2005) investigated one of the weak-lined T Tauri star (WTTS), MN Lupi in order to tell the spectral signatures of the accretion flow from the chromospheric and photospheric magnetic activity. They obtained Doppler images of hot spots at high stellar latitude and related it to the accretion shocks produced by the disk material funneling along the magnetic field lines. Donati et al. (2011) studied one of the CTTSs, TW Hya, and recently reported the results of spectropolarimetric observations. They observed a near-polar region of accretion-powered excess Ca II and He I emission which coincides with the main magnetic pole of TW Hya and they claimed that the accretion occurs mostly polewards at the stellar surface.

Many numerical simulations have also been made of accretion onto a magnetized star (e.g., Miller & Stone 1997; Romanova et al. 2002, 2011; Kulkarni & Romanova 2005; Long et al. 2008). Romanova et al. (2002) investigated disk accretion onto a rotating magnetized star and the associated funnel flows by performing a set of simulations for different stellar magnetic moments and rotation rates. In their investigation, they found that the dominant force driving plasma into FF is the pressure gradient force. Although they made numerical applications to T Tauri stars only, they claimed that their results are also valid for cataclysmic variables and neutron stars in X-ray binaries. Romanova et al. (2011) also performed axisymmetric MHD simulations of accretion onto magnetized stars from magnetorotational instability (MRI)-driven disks. Close to the star, they observed that the disk is stopped by the magnetic pressure of magnetosphere and matter is lifted through a funnel stream.

Plasma entry into magnetospheres is generally explained by plasma instabilities at the disk-magnetosphere interface in the radial flow case. A Rayleigh-Taylor instability is expected to occur at the interface, since the

magnetic field may act as a light fluid supporting a heavy fluid, i.e. plasma (Elsner & Lamb 1977, Arons & Lea 1976). In addition, the Kelvin-Helmholtz instability is expected to have a role in plasma entry, because of the relative motion of the plasma with respect to the magnetosphere (Arons & Lea 1976). Plasma entry via diffusion, magnetic reconnection and loss-cone mechanism have also been discussed by Elsner & Lamb (1984). Varniere & Tagger (2002) studied the accretion-ejection instability in magnetized disks. The authors claim that the instability can produce slow magnetosonic waves and they expect that these waves will lift the plasma above disk. Recently, Fu & Lai (2012) studied the dynamics of the innermost accretion flows around compact objects. Their investigation includes a comprehensive study of the large scale Rayleigh-Taylor and Kelvin-Helmholtz instabilities associated with the disk-magnetosphere interface of a rotating magnetized system.

The goal of this paper is to present the role of MRI in the interaction between the inner disk and the magnetosphere of CTTs. Balbus & Hawley (1991, hereafter BH91) showed that Keplerian disks with a weak field which fulfills the frozen in condition are dynamically unstable. If the magnetic field is weak, the perturbations generate an unstable mode which is non-propagating and evanescent. The importance of MRI lies in the generality in its applicability. After BH91 established the importance of MRI in the dynamics of the accretion disks, this instability has been received much attention and studied by many investigators over the last two decades. Most of these authors drew attention on the necessity of considering the non-ideal MHD effects in protoplanetary disks (PPDs). For example, Wardle (1999) found that the Hall effect modifies the growth rate of the instability. When the Hall current is dominated by the negative (positive) species, the parallel case becomes less (more) unstable. Balbus & Terquem (2001) analysed the Hall effect in protostellar disks and found that the inclusion of the Hall effect destabilizes the disk with any differential rotation law. Rüdiger & Shalybkov (2004) investigated the linear instability in a magnetic Taylor-Couette (TC) flow with Hall effect. One of the major conclusions they had drawn was that while the shear in disk is negative, the Hall instability combines with the MRI. Although their main interest was the TC flow they also commented on the Hall effect on the MRI in astrophysical objects (white dwarfs, neutron stars and protoplanetary disks).

More recently, Armitage (2011) argued that since the gas in PPDs is cool, dense and has a very low ionization fraction, one needs to take into consideration the non-ideal MHD effects, like Ohmic resistivity, Hall effect and ambipolar diffusion. Besides, these non-ideal terms are effective at different radial and vertical distances (z) in the disk. In that part of the disk where magnetic field is strongly coupled to electrons but not to the ions, the Hall effect is the most important one (Armitage 2011). He also clearly states that the conductivity and ionization fraction of the innermost disk fluid are high. Thus, non-ideal MHD effects play an important role at transporting angular momentum outward. Under these conditions the disk fluid interacts with the stellar magnetosphere and MRI is highly likely to set in. One of the most important conclusions Armitage (2011) draws is the absence of the non-linear solutions covering the non-ideal conditions, the Hall effect and the Ohmic and ambipolar diffusion in PPDs. He points to the future works which are to take into account of the global effects over long time scales. Besides, Bai (2011) investigated the MRI-driven accretion in protoplanetary disks (PPDs) by considering the non-ideal MHD effects including the Ohmic resistivity, the Hall effect and the ambipolar diffusion. Bai (2011) also warns the reader about the necessity of careful exploration of the Hall regime with numerical simulations which is yet to be done. If the Elsasser

number, which measures the relative importance of the Lorentz force and the Coriolis force is less than unity, then the non-ideal MHD terms dominates in the MRI active region and the linear properties of MRI change considerably (Bai 2011). In this region, the Hall effect and the ambipolar diffusion are the dominant ones. In our investigation we take only the Hall effect into consideration.

In the present investigation we are interested in the diamagnetic effect and its consequences as the gradient in the magnetic field and the perpendicular velocity (to the magnetic field) at the disk-magnetosphere boundary of CTTS. We investigate the instability of the mode with a wave vector perpendicular to the disk. We improve a model including the effect of diamagnetism on numerical growth rates of the unstable mode. The paper is structured as follows: In the following section, we briefly review the diamagnetic behaviour of the disk, then we present the mathematical formalism of diamagnetism. We also present the linearized form of the basic MHD equations and obtain the general form of the dispersion relation in section 2. In section 3, a detailed analysis of the effect of the magnetic field and perpendicular velocity gradients produced by magnetization on the numerical growth rates of the unstable mode is carried out. Finally in section 4, we summarize our conclusions from this work.

2. Basics

2.1. Theoretical background on diamagnetism

The diamagnetic effect arises when particles moving in an external magnetic field create their own field. In this investigation, we assume that the charged particles are frozen into the magnetic field. If charged particles gyrating around the magnetic field lines produce a net current at the boundary of a closed circuit, this current in turn produces a new magnetic field (Singal 1986, Bodo et al. 1992). The direction of this new and local magnetic field will be the same as the global magnetic field outside the circuit and the opposite within the circuit. The net magnetic field inside the region will therefore be lower than that of outside and a gradient in the magnetic field will be produced. Electrically charged particles gyrating under the influence of “ ∇B ” and “ $\nabla \times \vec{B}$ ” will give rise to a drift current at the border of the region (see Fig.1). Because the magnetic moment ($\mu = mv_{\perp}^2/2B$), the first adiabatic invariant is conserved, we expect the magnetic field gradient to produce a gradient in the perpendicular velocity (v_{\perp}) of the particles.

The counterfield produced by particles can be expressed by magnetization, defined as the magnetic moment per unit volume (Singal 1986):

$$\mathbf{M} = \int_{4\pi} \int_0^{\infty} N(E, \theta) \mu(E, \theta) dE d\Omega. \quad (1)$$

Here, $N(E, \theta) dE d\Omega$ is the number density of charged particles having velocity within $d\Omega$ around pitch angle θ and energy within dE around E . By using the definition of the magnetic moment, the magnetization is found as

$$\mathbf{M} = -\frac{\mathbf{B}}{3B^2} (W_r + 2W_{nr}) \quad (2)$$

where W_r and W_{nr} are the energy densities of the relativistic and non-relativistic particles, respectively (Singal 1986; Bodo et al.1992). In our investigation we discarded the relativistic electrons flowing in the currents. Therefore, Eq. (2) can be rewritten in terms of the perpendicular component of the kinetic energy density of non-relativistic electrons as

$$\mathbf{M} = -\frac{2\mathbf{B}}{3B^2}W_k \quad (3)$$

where $W_k = nmv_{\perp}^2/2$, with n the particle density. In the close neighborhood of the magnetization current carrying circuit, the net magnetic field may be written as

$$\mathbf{B} = \mathbf{H} + 4\pi\mathbf{M} = \mathbf{H} - \frac{8\pi}{3} \frac{\mathbf{B}}{B^2}W_k = \mathbf{H} - \frac{1}{3} \frac{W_k}{W_B}\mathbf{B} = \mathbf{H} - \varepsilon\mathbf{B} \quad (4)$$

where $W_B = B^2/8\pi$ is the magnetic field energy density and $\varepsilon = W_k/3W_B$, which is called the ‘‘magnetization parameter’’in Devlen & Pekünlü (2007, hereafter DP07).

In the presence of diamagnetism, the total current density may be written as

$$\mathbf{J} = \mathbf{J}_{\text{ext}} + \mathbf{J}_{\text{mag}} = \frac{c}{4\pi}\nabla \times \mathbf{H} + c\nabla \times \mathbf{M} = \frac{c}{4\pi}\nabla \times \mathbf{H} - c\nabla \times \frac{2W_k}{3B^2}\mathbf{B}. \quad (5)$$

After some vector operations the current density is found as below (DP07):

$$\mathbf{J} = \frac{c}{4\pi} \left[(1 - \varepsilon)\nabla \times \mathbf{B} + 2\varepsilon \frac{\nabla B}{B} \times \mathbf{B} - 2\varepsilon \frac{\nabla v_{\perp}}{v_{\perp}} \times \mathbf{B} \right]. \quad (6)$$

MRI is shown to be the source of turbulence in disks (BH91, Balbus & Hawley 1998, hereafter BH98). If fluid elements with outwardly decreasing velocity field couple with the magnetic field then a torque is produced which causes enhanced outward angular momentum transport.

In the present study, we intend to seek a solution to the cause of funnel flow departing from the inner boundary of the disk. The equilibrium magnetic field at the above mentioned location is assumed to be in the z -direction and perpendicular to the disk. If the angular velocity of the inner portion of the differentially rotating disk is more or less equal to that of the last closed field line of the co-rotating magnetosphere, we may expect the disk material be trapped at this border. Then, the positively and the negatively charged particles will acquire drift velocities in the opposite senses perpendicular to the local magnetic field due to the curl and the gradient of the dipole magnetic field, the latter of which is inversely proportional to the third power of the radial distance. This will bring about a local current flowing at the border of the inner disk and the co-rotating magnetosphere. This local current will generate its own magnetic field in such a way as to increase the magnetic field intensity outside and to decrease it inside the circuit. So called diamagnetic effect will generate a magnetic field gradient in the radial direction. The weaker magnetic field, necessary for the MRI to set in, within the circuit may trigger the perturbations at the border. If the gradient of the magnetic field is steep enough then the magnetic pressure force will be exerted upon the disk material in the negative radial direction. Assuming that the diamagnetic current lasts long enough to maintain the magnetic field gradient which through the magnetic pressure force pushes the disk material into the diamagnetic current

circuit and thus the condition between the sound speed (c_s) and the Alfvén speed (v_A), $c_s^2 > v_A^2$ is fulfilled which is a necessary condition for MRI to set in.

The magnetic field which was in the z-direction at equilibrium, now, by the push of the frozen-in trapped particles at the neighbourhood of the border will acquire a curly shape. Contribution to the drift velocity, originally produced by the magnetic field gradient, of the electrons from the curvature of the field lines will enhance the diamagnetic current which in turn weakens the magnetic field within the circuit. This is an additional agent to cause MRI to set in. The direction of the electron drift velocity is in the opposite sense to the motion induced by the stabilizing Coriolis force (see, e.g. DP07). The frozen-in electrons' motion which has destabilizing effect on the disk fluid is in the same sense of the induced whistler circular motion of the field lines (Balbus & Terquem 2001, hereafter BT01). It was pointed out by BT01 and DP07 that the drifting electrons impart a circularly polarized component to the velocity response which damps the Coriolis force and suppresses the stabilizing dynamical epicyclic motion.

In the analysis of the diamagnetic effect on MRI, DP07 found that the magnetic field gradient generated by the magnetization current produces a new unstable mode. They also showed that the maximum growth rates and the parameter spaces for the unstable modes depend strongly on the magnitude of the magnetization and the magnetic field gradient it produces. In their investigation, they assumed that the perpendicular velocity v_\perp does not vary in space around the fiducial radius R. Therefore, they consider the effect of magnetic field gradient only. Formally speaking, they dropped the third term on the right-hand side of Eq. (6) containing ∇v_\perp . In this study, we will include the effects of both the magnetic field and perpendicular velocity gradients for the first time.

2.2. The geometry of disk-magnetosphere boundary

We assume a differentially rotating disk which manifests itself in $\kappa (=4\Omega^2 d\Omega^2/d \ln R)$ epicyclic frequency and the dimensionless parameter $T (=d \ln \Omega^2/d \ln R)$ where Ω is the angular velocity of the disk. Next, we also assume that the disk fluid to be coupled to the weakly magnetized disk. These two assumptions indicate that if an instability arises it is highly likely to be MRI. We have taken neither self-gravity of the disk nor the gravitational force of the CTTS into account. Otherwise, one may argue the role of Rayleigh-Taylor instability. The kinetic energy of the relative motions of drifting electrons and positively charged particles is fed into a plasma wave of the suitable phase velocity. The amplitude of this properly selected wave may grow and result in instability (Somov 2006). We assume that the last closed field lines co-rotate both with the star and the inner boundary of the accretion disk. If this assumption is justifiable then we may proceed as follows. Since the disk fluid at the inner boundary is expected to be highly ionized and transfer angular momentum outwards from the star, particles move inward (BH91, BH98). They eventually become trapped in the magnetosphere of the star and simultaneously acquire drift velocities. Due to the curvature and the gradient of the magnetic field, electrons and positively charged particles drift in the opposite directions and thus produce a current flowing along the inner boundary, just like the ring current that flows in the terrestrial magnetosphere. This current generates its own magnetic field and causes diamagnetism at the

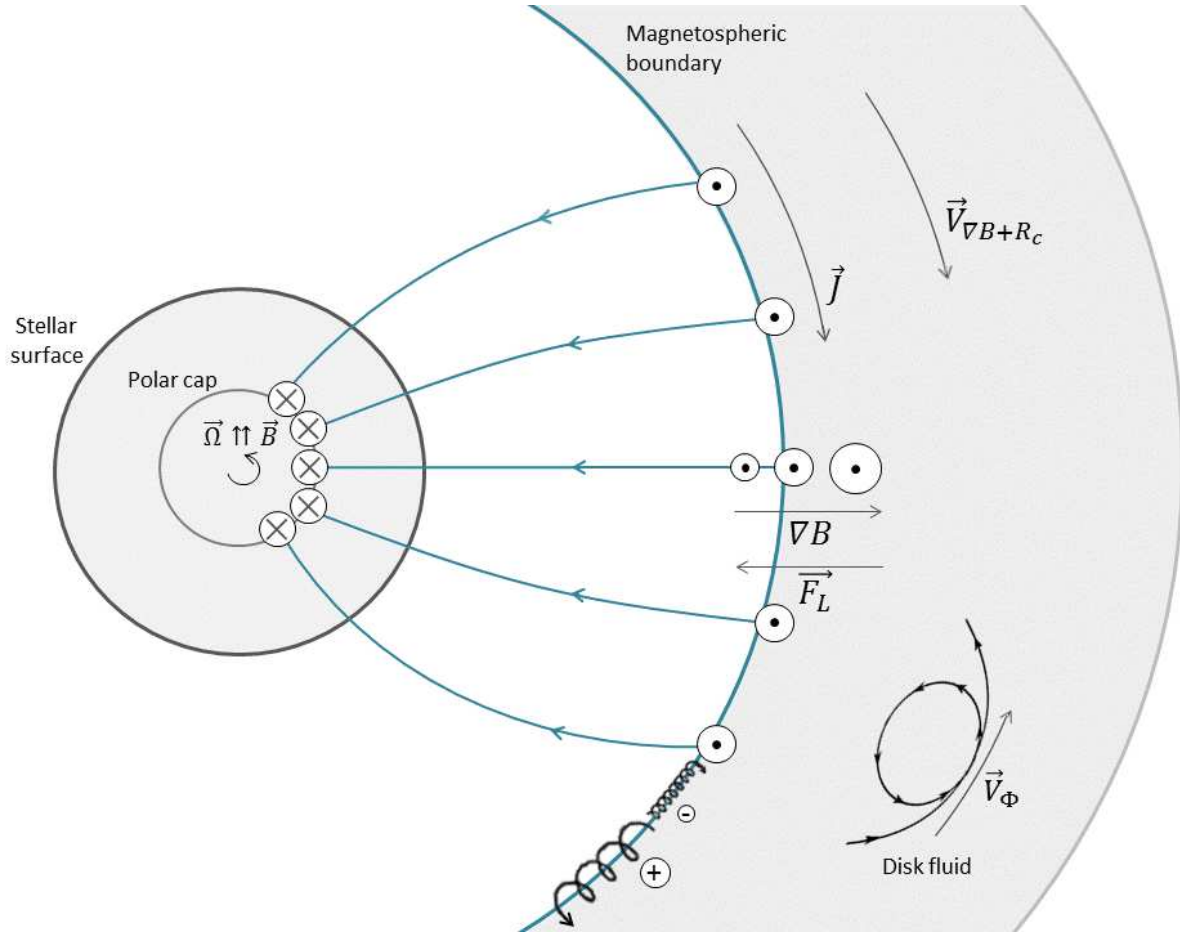


Fig. 1.— Top view of the border between the inner magnetosphere and the accretion disk (not to scale). Symbols \odot and \otimes represent the magnetic field vectors opposite and the same direction to the los respectively. Cycloids at the inner radius of the disk represent the electron and proton trajectories. Drift motions of the trapped particles with a velocity $\vec{V}_{\nabla B + R_c}$ generate diamagnetic current \vec{J} . This current produces its own magnetic field in such a way as to produce a magnetic field gradient ∇B at the border. Generated magnetic pressure force combined with the tension force due to the curved field lines exert Lorentz force \vec{F}_L to the particles. Epicyclic motion of the disk fluid is also shown at the bottom right of the figure.

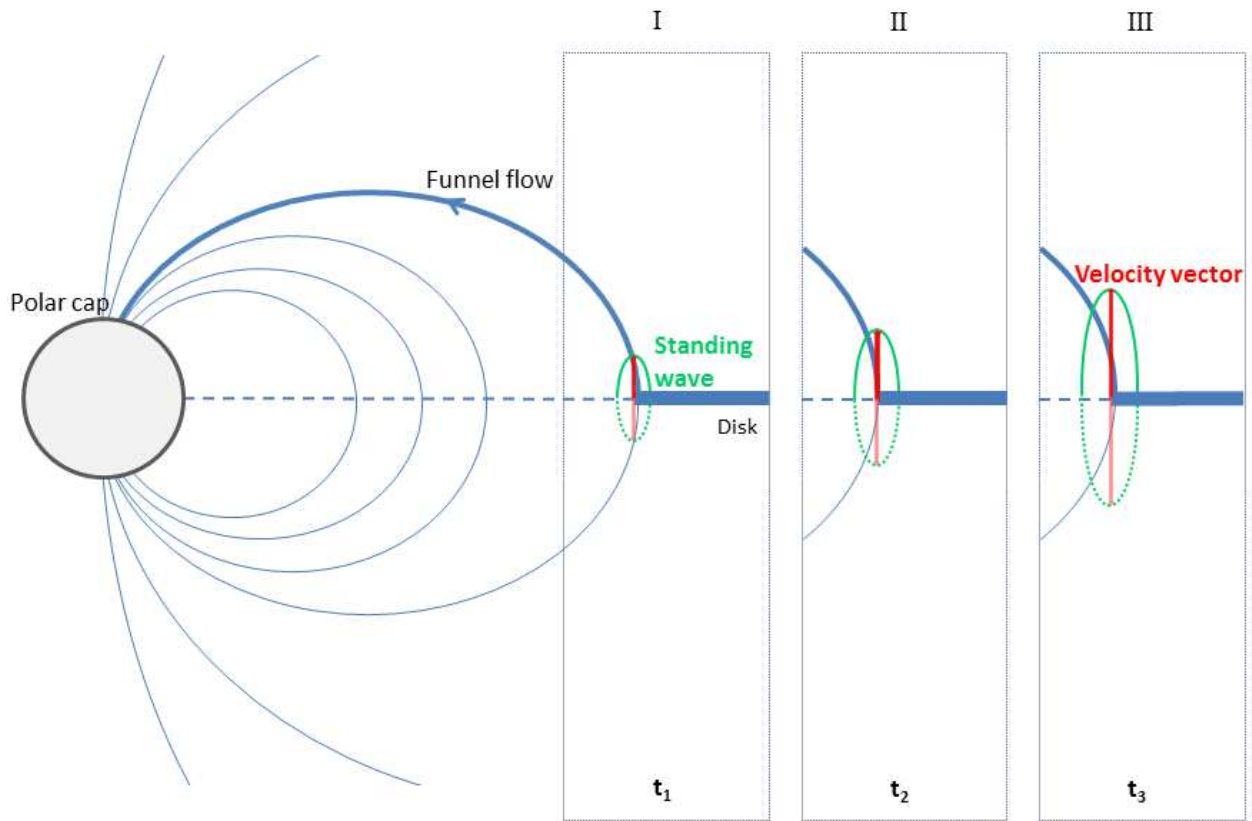


Fig. 2.— The inner boundary of the accretion disk is assumed to be co-rotating with the last closed field line of the magnetosphere. The amplitude of an unstable standing wave which is generated by *diamagnetic current modified MRI* at this border grows by time (see section 3) and pushes the disk fluid along the magnetic field lines with approximately zero pitch angle. As a result of this combination, i.e., gravitational pull by the central object and magnetic field guidance, funnel flow towards the magnetic polar regions becomes possible. Growing unstable wave amplitude is represented by a sinusoidal curve. As the unstable standing wave amplitude grows, disk fluid is channeled upward (continuous curve) and downward (dotted curve) directions towards the magnetic polar regions.

inner disk boundary. The width of the region where this current flows is of the order of the ions' average Larmor radius ($r_L = mv_{\perp}c/qB$) which is found to be 200 cm for CTTS. The net magnetic field within that part of the magnetosphere that is neighboring the diamagnetic current circuit is weaker than that of just outside the current carrying circuit. Thus, a gradient of a magnetic field is produced across the disk-magnetosphere boundary pointing radially out from the star. If we assume that the magnetic moment, ($\mu = mv_{\perp}^2/2B$) is conserved for the particles, the particles' perpendicular velocities, vary while they enter into and exit from the higher magnitude field regions.

When the magnetic and rotation axes are not aligned, the drifting disk fluid particles will spend half the *drift period* on the northern magnetic hemisphere and the other half on the southern one. Let us try to depict the magnetic course of the drifting particles. We assume that positively charged particles, starting from the magnetic equator, are drifting towards the magnetic northern latitudes. They would encounter higher and higher magnetic field intensity through a *quarter-drift-period* (*qdp*). The next *qdp* would be the time to descend towards the magnetic equator. The drifting particles would encounter a similar ascend and descend towards the southern magnetic pole at the second half of the *drift period*. During this periodic ascending and descending from the magnetic polar regions, drifting particles would encounter magnetic field gradients in the azimuthal direction, in addition to the radial one generated by the diamagnetic current. In this study, we will not consider the non-aligned case and will put it off until a future study.

Let us consider a simple case wherein the rotation axis and the magnetic moment axis are coincident, i.e., $\vec{\Omega} \uparrow \uparrow \vec{B}$ (see Fig. 1). In the *top view* outer circle represents the CTTS projected on a (R, ϕ) plane in cylindrical coordinates; inner circle represents the latitude of the last closed field lines on the star. The innermost circular arc is the inner boundary of the disk; the symbols \odot and \otimes stand for the magnetic field vectors the directions of which are the opposite and the same, respectively, to the *los* of the reader. Cycloid which is not drawn to the scale represents the stabilizing epicyclic motions of the disk fluid. Diamagnetic current produced magnetic field adds to the stellar field outside the circuit and subtracts at the inside and thus brings about a magnetic field gradient which points in the R direction. The Lorentz force due to the magnetic pressure is in the negative R direction. At the same location, the direction of the magnetic tension force is also in the negative R direction and thus net force is strengthened.

If the drift velocity, $V_{\nabla B+R_c} \propto R_c \times B$ where R_c is the radius of curvature of the magnetic field at the inner border of the disk, persists which in turn keeps the diamagnetic current flow in the same sense as the induced whistler circular motion then the diamagnetic effect destabilizes the disk just like the whistler circular motion (DP07).

Diamagnetic-current-producing drifts may be described as a self-organization process. It is argued that these kind of processes keep their presence even at the turbulent stage (e.g. Fridman et al. 2006, Prigogine & Stengers 1984). disk-magnetosphere interaction region may be defined as an open non-linear magnetohydrodynamic system. This system can generate macroscopic dissipative structures with various spatial and temporal scales by an internal self organization like diamagnetic current. One may argue that this current can maintain itself even at the onset of the turbulence. But here, we make no claims as to the nonlinear regime which is to be explored by numerical simulations. Our argument about the diamagnetic

currents is valid only in the linear regime.

Finally, let us imagine a slow and/or standing unstable wave produced at the inner edge of the disk (see Fig. 2). In the next section we will show that the solution of the dispersion relation reveals the existence of an unstable standing wave. Therefore we deem it necessary to visualize the physical process at the disk-magnetosphere boundary by drawing the Fig. 2. The disk fluid is forced by gravity which manifests itself by Keplerian velocity profile, towards a CTTS and guided by the magnetic field. Now, the growing amplitude of the unstable mode is highly likely to push the disk matter parallel to the local magnetic field lines, i.e., with an approximately zero pitch angle. This means that species of the disk fluid, under this condition, will seek their respective mirror points at the stronger parts of the magnetic field and eventually hit the magnetic polar regions.

If the above assumptions we make are justifiable then we expect the physical processes described above to take place. The different drift velocities acquired by electrons and ions may bring about the Hall currents as well. By taking into account all these probabilities we set ourselves to the task of investigating the possible role of MRI in producing slow or standing wave modes which may guide the disk fluid along the magnetic field lines and thus cause the precipitation of the plasma towards the magnetic poles of the star.

2.3. Equations

The fundamental equations are mass conservation, the equation of motion and the induction equation, given below, respectively:

$$\frac{\partial \rho}{\partial t} + \nabla \cdot (\rho \mathbf{v}) = 0 \quad (7)$$

$$\rho \frac{\partial \mathbf{v}}{\partial t} + (\rho \mathbf{v} \cdot \nabla) \mathbf{v} = -\nabla P + \frac{1}{c} \mathbf{J} \times \mathbf{B} \quad (8)$$

$$\frac{\partial \mathbf{B}}{\partial t} = \nabla \times \left[\mathbf{v} \times \mathbf{B} - \eta \frac{4\pi}{c} \mathbf{J} - \frac{\mathbf{J} \times \mathbf{B}}{en_e} \right]. \quad (9)$$

Current density (\mathbf{J}) which is given by Eq. (6) will be substituted into Eqs. (8) and (9) in order to analyse the influence of the diamagnetism on MRI. As a result, the equations of modified momentum conservation and magnetic induction turn out to be

$$\rho \frac{\partial \mathbf{v}}{\partial t} + (\rho \mathbf{v} \cdot \nabla) \mathbf{v} = -\nabla P + \frac{1}{4\pi} \left[(1 - \varepsilon) (\nabla \times \mathbf{B}) \times \mathbf{B} + 2\varepsilon \left(\frac{\nabla B}{B} \times \mathbf{B} \right) \times \mathbf{B} - 2\varepsilon \left(\frac{\nabla_{\perp} \mathbf{v}}{v_{\perp}} \times \mathbf{B} \right) \times \mathbf{B} \right] \quad (10)$$

$$\frac{\partial \mathbf{B}}{\partial t} = \nabla \times \left[\begin{array}{l} \mathbf{v} \times \mathbf{B} - \eta(1 - \varepsilon) \nabla \times \mathbf{B} - 2\varepsilon\eta \frac{\nabla B}{B} \times \mathbf{B} + 2\varepsilon\eta \frac{\nabla v_{\perp}}{v_{\perp}} \times \mathbf{B} - (1 - \varepsilon) \frac{c(\nabla \times \mathbf{B}) \times \mathbf{B}}{4\pi en_e} \\ -2\varepsilon \frac{c}{4\pi en_e} \left(\frac{\nabla B}{B} \times \mathbf{B} \right) \times \mathbf{B} + 2\varepsilon \frac{c}{4\pi en_e} \left(\frac{\nabla v_{\perp}}{v_{\perp}} \times \mathbf{B} \right) \times \mathbf{B} \end{array} \right]. \quad (11)$$

We consider the local stability of a differentially rotating disk threaded by a vertical field with a gradient in the radial direction, $\mathbf{B} = B(R)\hat{z}$. Therefore the gradient of the magnetic field can be expressed by $\nabla B = (dB/dR)\hat{\mathbf{R}}$. The perpendicular velocity of the particles also has a gradient in the radial direction, i.e. $\nabla v_{\perp} = (dv_{\perp}/dR)\hat{\mathbf{R}}$. We assume that finite resistivity and Hall currents are both present. We shall work in the Boussinesq limit. The Boussinesq approximation is frequently used in descriptions of the nature of accretion disk transport. For instance, BH98 argue that velocity field in accretion disks may be taken as incompressible ($\nabla \cdot \mathbf{u} = 0$) for the turbulent flows. They also warn the reader that the disk fluid “is not exactly but nearly” incompressible. In detail, they say that $(\nabla \cdot \mathbf{u})^2$ is negligible compared to $|\nabla \times \mathbf{u}|^2$ and also $\nabla(\nabla \cdot \mathbf{u})$ is negligible compared to $\nabla^2 \mathbf{u}$, but $P \nabla \cdot \mathbf{u}$ is to be kept in the thermal equation. This is how the Boussinesq approximation defined in the context of accretion disks. We use standard cylindrical coordinates (R, ϕ, z) with the origin at the disk center. Finally, we assume that the perturbed quantities’ variation in space and time is like a plane wave, i.e., $\exp(ikz + \omega t)$, where k is the wave number perpendicular to the disk and ω is the angular frequency. This form keeps the coefficients of the dispersion relation real and a positive real root ω implies unstable exponential growth of the mode. Since we are interested in plasma motion perpendicular to the disk plane, we investigate the instability of the mode with a wave vector perpendicular to the disk. Under these circumstances, the linearized form of Eq. (7), (10) and (11) are found as:

$$\omega \delta v_R - 2\Omega \delta v_{\phi} - (1 - \varepsilon) \frac{ik_z}{4\pi\rho} B_z \delta B_R + \frac{1}{4\pi\rho} \left[(1 + 3\varepsilon) \nabla B - 4\varepsilon B_z \frac{\nabla \Omega}{\Omega} \right] \delta B_z = 0 \quad (12)$$

$$\omega \delta v_{\phi} + \frac{\kappa^2}{2\Omega} \delta v_R - (1 - \varepsilon) \frac{ik_z}{4\pi\rho} B_z \delta B_{\phi} = 0 \quad (13)$$

$$\frac{ik_z \delta P}{\rho} - \frac{1}{4\pi\rho} \left[(1 + \varepsilon) \nabla B - 2\varepsilon B_z \frac{\nabla \Omega}{\Omega} \right] \delta B_R = 0 \quad (14)$$

$$ik_z B_z \delta v_R - \left[\omega + \eta(1 - \varepsilon) k_z^2 \right] \delta B_R - (1 - \varepsilon) \frac{c}{4\pi en_e} B_z k_z^2 \delta B_{\phi} = 0 \quad (15)$$

$$\begin{aligned} & \left\{ \frac{d\Omega}{d \ln R} + \frac{c}{4\pi en_e} \left[(1 - \varepsilon) k_z^2 B_z + (1 + \varepsilon) \nabla^2 B - 2\varepsilon \left(B_z \frac{\nabla^2 \Omega}{\Omega} + \nabla B \frac{\nabla \Omega}{\Omega} - B_z \left(\frac{\nabla \Omega}{\Omega} \right)^2 \right) \right] \right\} \delta B_R \\ & - \left[\omega + \eta(1 - \varepsilon) k_z^2 - 2\varepsilon \eta \left(\frac{\nabla^2 B}{B} - \left(\frac{\nabla B}{B} \right)^2 - \frac{\nabla^2 \Omega}{\Omega} + \left(\frac{\nabla \Omega}{\Omega} \right)^2 \right) \right] \delta B_{\phi} \\ & + ik_z B_z \delta v_{\phi} + \frac{c}{4\pi en_e} 2\varepsilon \left[ik_z \nabla B - ik_z B_z \frac{\nabla \Omega}{\Omega} \right] \delta B_z = 0 \end{aligned} \quad (16)$$

$$\begin{aligned} & \nabla B \delta v_R + 2\varepsilon \eta i k_z B_z \frac{\nabla \Omega}{\Omega} \delta v_\phi - \frac{c}{4\pi e n_e} \left[(1 + \varepsilon) i k_z \nabla B - 2\varepsilon i k_z B_z \frac{\nabla \Omega}{\Omega} \right] \delta B_\phi \\ & - \left[\omega + \eta(1 - \varepsilon) k_z^2 + 2\varepsilon \eta \left(i k_z \frac{\nabla B}{B} - \frac{\nabla^2 B}{B} + \left(\frac{\nabla B}{B} \right)^2 - \frac{\nabla^2 \Omega}{\Omega} + \left(\frac{\nabla \Omega}{\Omega} \right)^2 \right) \right] \delta B_z = 0. \end{aligned} \quad (17)$$

where $\kappa = 4\Omega^2 d \Omega^2 / d \ln R$ is the epicyclic frequency and Ω is the angular velocity of the disk. The linearized Eqs. (12)-(17) give a 5th-order dispersion relation that emerges after a very lengthy effort. This describes five low-frequency modes. However, in the limit of zero resistivity, the analysis is reduced to finding the roots of a quartic. In this case, the dispersion relation in dimensionless form is found as

$$s^4 + \mathcal{C}_2 s^2 + \mathcal{C}_0 = 0 \quad (18)$$

where $s = \omega/\Omega$. The coefficients \mathcal{C}_2 and \mathcal{C}_0 are found as follows:

$$\begin{aligned} \mathcal{C}_2 = & \tilde{\kappa}^2 + 2X(1 - \varepsilon) + \frac{Y}{4}(1 - \varepsilon)[Y(1 - \varepsilon) + T] + G^2 M_A^{-2} [(1 + 3\varepsilon) - \chi Y \varepsilon(1 + \varepsilon)] \\ & + \frac{3}{4} G T M_A^{-2} \chi Y \varepsilon(1 + 3\varepsilon) + \frac{T^2}{8} M_A^{-2} \chi Y \varepsilon(8 - 9\varepsilon) \end{aligned} \quad (19)$$

$$\begin{aligned} \mathcal{C}_0 = & G^2 M_A^{-2} \left\{ (1 - \varepsilon) \left[X(1 + 3\varepsilon) + 4\chi X \varepsilon + \frac{Y^2}{2}(1 - \varepsilon) \right] + (1 + \varepsilon) \chi \tilde{\kappa}^2 \left[Y \varepsilon - \frac{X}{4}(1 + 3\varepsilon) \right] \right\} \\ & + G T M_A^{-2} \left\{ \begin{aligned} & \frac{\chi}{2} \tilde{\kappa}^2 (X - Y) \varepsilon(1 + \varepsilon) - 2(3\chi - 2) \varepsilon(1 - \varepsilon) \\ & - \frac{\chi}{8} X T \varepsilon(7 + 5\varepsilon) + \frac{Y^2}{4} \varepsilon^2(1 - \varepsilon)^2 + \frac{\chi}{2} X G(1 + 3\varepsilon)(1 + \varepsilon) \\ & + M_A^{-2} \chi Y \left[\frac{G T}{4} \varepsilon^2(1 + 3\varepsilon) - 2\varepsilon(1 - \varepsilon) - \frac{T^2}{8} \varepsilon^2(11 + 3\varepsilon) - \frac{G^2}{2} \varepsilon(1 + 3\varepsilon) \right] \end{aligned} \right\} \\ & - T^2 M_A^{-2} \left\{ \begin{aligned} & \frac{\chi}{8} Y \tilde{\kappa}^2 \varepsilon(1 + 3\varepsilon) + \frac{\chi}{2} X \varepsilon \left[(1 - \varepsilon) - \tilde{\kappa}^2 \varepsilon + T \varepsilon \right] \\ & + \frac{\chi}{4} M_A^{-2} \varepsilon^2 \left[T^2 \varepsilon^2 + 2(1 - \varepsilon) \right] - \frac{Y^2}{8} \varepsilon^2(1 - \varepsilon) \end{aligned} \right\} \\ & + \left[T(1 - \varepsilon) + Y(1 - \varepsilon)^2 + X(1 - \varepsilon)^2 \right] \left(\frac{\tilde{\kappa}^2 Y}{4} + X \right). \end{aligned} \quad (20)$$

Here the dimensionless parameters are defined as $s = \omega/\Omega$, $X = (k v_A/\Omega)^2$, $Y = (k v_H/\Omega)^2$, $\tilde{\kappa} = \kappa/\Omega$, $G = d \ln B/d \ln R$, $T = d \ln \Omega^2/d \ln R$ and $\chi \equiv v_H^2/v_A^2$. The Hall and the Alfvén speeds are defined as $v_H^2 = \Omega B c / 2\pi e n_e$ and $v_A^2 = B^2 / 4\pi \rho$. The Alfvén Mach number of Keplerian (orbital) motion $M_A = v_\phi / v_A$ measures the relative strength between the kinetic energy and the magnetic energy. We can rewrite the Alfvén Mach number in terms of ε as $M_A^2 = 3\varepsilon$.

In this case, the dispersion relation gives two fast and two slow modes which are labeled depending on the magnitude of their phase velocities. Besides, in Figs. 3-5 which are given in the next section, ridges of the growth rates correspond to the sites (in X,Y) of standing waves, i.e., the solution of dispersion relation gives real ω . No harm in repeating that we assumed the phasor factor of the waves as $\exp(ikz + \omega t)$. Therefore, the slow mode turns into non-propagating, i.e. standing mode in the (X,Y) regions of instability, since $\omega_i = 0$. disk fluid will be pushed up and down along the magnetic field while the magnitude of the standing wave grows through instability. This, we believe, is the way to lift the material from the disk into funnel flow. The disk material gains momentum in this way and enters into the magnetic field with almost zero pitch angle and be guided towards the magnetic poles of the star under gravitational force.

We seek the solution at a fiducial radius (R). In this investigation, the fiducial radius corresponds to the close neighbourhood of the *Alfvén radius* where plasma pressure is slightly bigger than the magnetic pressure.

Eq. (18) is the general form of the dispersion relation, wherein the gradient in the magnetic field (∇B) and the perpendicular velocity (∇v_{\perp}) are both considered. This amounts to saying that the magnetization currents are persistent and strong in the disk-magnetosphere boundary. Therefore, the long-lasting currents can produce a gradient in the magnetic field and perpendicular velocity in turn. In the next section, we will compare our results for three cases: *i*) $\nabla B = 0, \nabla v_{\perp} = 0$; *ii*) $\nabla B \neq 0, \nabla v_{\perp} = 0$; *iii*) $\nabla B \neq 0, \nabla v_{\perp} \neq 0$.

3. Numerical Growth Rates of the Unstable Mode

The graphical solutions of Eq. (18), the numerical growth rates (s), are thus shown in (X,Y) plane in Figs. (3)-(5). Here we present the results for three cases. First we assume that the magnetization current is not persistent but fluctuates, so that the magnetic field and perpendicular velocity gradients produced at the disk-magnetosphere boundary can be neglected. Formally speaking, the second and the third term on the right-hand side of Eq. (6) will be dropped, i.e. $\nabla B = 0$ and $\nabla v_{\perp} = 0$. Then, we consider a long-lasting current and take the magnetic field gradient into account, but the perpendicular velocity still remains constant in space around the fiducial radius R , i.e. $\nabla B \neq 0$ and $\nabla v_{\perp} = 0$. Finally, we consider the effects of both the magnetic field and perpendicular velocity gradients, i.e. $\nabla B \neq 0$ and $\nabla v_{\perp} \neq 0$. Therefore we can compare the results for these three cases.

BT01 discussed the Hall effect on MRI in protostellar disks from a dynamical point of view. Although they focused on protostellar disks only, they claimed that their results are broadly applicable. They analyzed the relative importance of the Hall term both for gases with a low-ionization fraction and for fully ionized plasma. One of the important conclusions of their analysis is that the temperature and density regimes of ionized accretion disks imply that the Hall effect cannot be ignored. Bearing this analysis in mind, we choose to take the Hall effect into account. We can estimate the Hall parameter for TT disks as follows: TT disks are expected to be truncated at distances of several stellar radii from the star (Johns-Krull 2007). Bouvier et al. (2007) found the truncation radius where the stellar magnetic field starts to control the motion of the accreting plasma as about 7 stellar radii for $B_* = 1$ kG. Then at $R_M = 7R_*$ the magnetic field strength is found as $B_M = B_*(R_*/R_M)^3 \approx 2.9$ G. Typical midplane gas density in TT disks is given as $\rho_g = 10^{-9}$ gcm $^{-3}$ (Alexander 2008). Glassgold et al. (2007) found the electron number density as 10^5 cm $^{-3}$ from Neon fine structure line emission of a TT disk. For a typical period $P \sim 8^d$, the χ value is found as 4. We will use this value for the Hall parameter in our numerical solutions.

3.1. Growth rates in case of $\nabla B = 0$ and $\nabla v_{\perp} = 0$

As we mentioned above, in our first solution (Solution I) we neglect the gradients of the magnetic field and the perpendicular velocity generated by the magnetization current at the disk-magnetosphere boundary.

Table 1: The maximum numerical growth rates found from Solution I and II.

		s_m			
		$\varepsilon = 0.1$		$\varepsilon = 0.5$	
		FUR	SUR	FUR	SUR
Solution I	G=0.0	0.75	-	0.75	-
Solution II	G=0.1	0.78	0.22	0.79	0.10
	G=0.5	1.37	1.02	1.58	0.82
	G=1.0	2.43	2.21	4.42	2.65

The Solution I ($G=0, T=0$) reveals one unstable region. The Solution II ($G \neq 0, T=0$) reveals two unstable regions. We label them as FUR (First Unstable Region), and SUR (Second Unstable Region).

Table 2: The maximum growth rates for Solution III.

		s_m	
		FUR	SUR
Solution III	G=0.1, $\varepsilon = 0.1$, T=-3	1.41	1.52
	G=0.5, $\varepsilon = 0.4$, T=-3.5	-	14.78
	G=1.0, $\varepsilon = 0.7$, T=-4	-	29.13

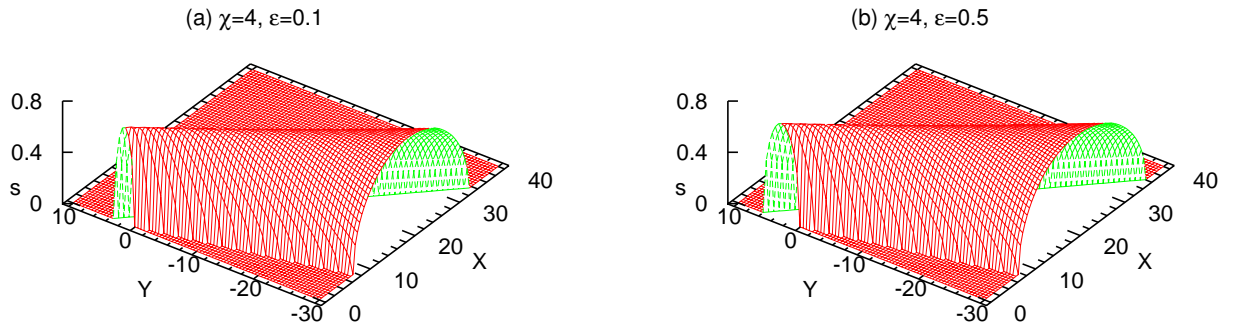


Fig. 3.— Growth rates found from Solution I. Only regions of instability are shown, with the height proportional to the growth rate. The regions of instability are seen as “ridges” above the X,Y plane (see text for definitions). The maximum growth rate of the “ridge” is 0.75 for both cases: (a) weak magnetization ($\varepsilon = 0.1$); (b) strong magnetization ($\varepsilon = 0.5$). However, the unstable region slightly widens with increasing ε .

We assume a uniform vertical magnetic field, $\mathbf{B} = B\hat{z}$.

The graphical solutions are given in Fig. 3. In order to see the effect of magnetization on growth rates, we plot our graphs for a weak ($\varepsilon = 0.1$) and strong ($\varepsilon = 0.5$) magnetization. For both cases, the maximum value of the growth rate is 0.75 and independent of the value of ε . However, it is apparent that the region of instability which is seen as a ridge, slightly widens when we increase the value of ε (see Fig. 3b).

We should mention that when $\varepsilon = 0$, the dispersion relation is reduced to Eq. (57) of BT01 and the graphs of Solution I are clearly similar to that of BT01, as they should be.

3.2. Growth rates in case of $\nabla B \neq 0$ and $\nabla v_{\perp} = 0$

In our second solution (Solution II), we consider a strong, long-lasting magnetization current that can produce a gradient in the magnetic field at the disk-magnetosphere boundary. The equilibrium vertical magnetic field is assumed to vary in the radial direction, i.e. $\mathbf{B} = B(R)\hat{z}$. Therefore the gradient of the magnetic field can be expressed by $\nabla B = (dB/dR)\hat{\mathbf{R}}$. We still assume that the perpendicular velocity does not vary in space at the disk-magnetosphere boundary (i.e. $\nabla v_{\perp} = 0$).

The results of Solution II are presented in Fig. 4. A new unstable region comes into existence with the inclusion of ∇B . From now on, we refer to this new region of instability as the *second unstable region* (SUR) and the one which was found in Solution I as the *first unstable region* (FUR). We again present the roots for a weak (see the left panel in Fig. 4) and strong (see the right panel in Fig. 4) magnetization respectively. In order to see the effect of ∇B on growth rate, we keep ε constant and change the value of G from arbitrarily chosen values of 0.1, 0.5 and 1. In Figs 4a, b and c, we keep $\varepsilon = 0.1$ and increase the value of G. It is apparent that when the value of G increases, the SUR becomes wider and the maximum value of the growth rates becomes higher. For G=1, the maximum growth rate which is included in the SUR, turns out to be 2.43 (see Fig. 4c). The maximum growth rates of the SUR and the FUR are listed in Table 1 for different values of ε and G. In Figs 4d, e and f we keep $\varepsilon = 0.5$ and increase the value of G again. When we compare the results for weak ($\varepsilon = 0.1$) and strong ($\varepsilon = 0.5$) magnetization, we see that the maximum values of the growth rates turn out to be higher in the presence of strong magnetization. The maximum growth rate reaches a value of 4.42 for G=1 and for $\varepsilon = 0.5$. The unstable regions (both FUR and SUR) again spread over a larger space in the X,Y plane for $\varepsilon = 0.5$ than they do for $\varepsilon = 0.1$.

We should mention that the results of Solution II are clearly similar to that of DP07, since the inclusion of magnetic field gradient is the same case considered in DP07. However, the maximum values of the growth rates are found to be slightly lower than that of DP07. This is highly probably a result of the Hall effect. The low value of the Hall parameter decreases the growth rates.

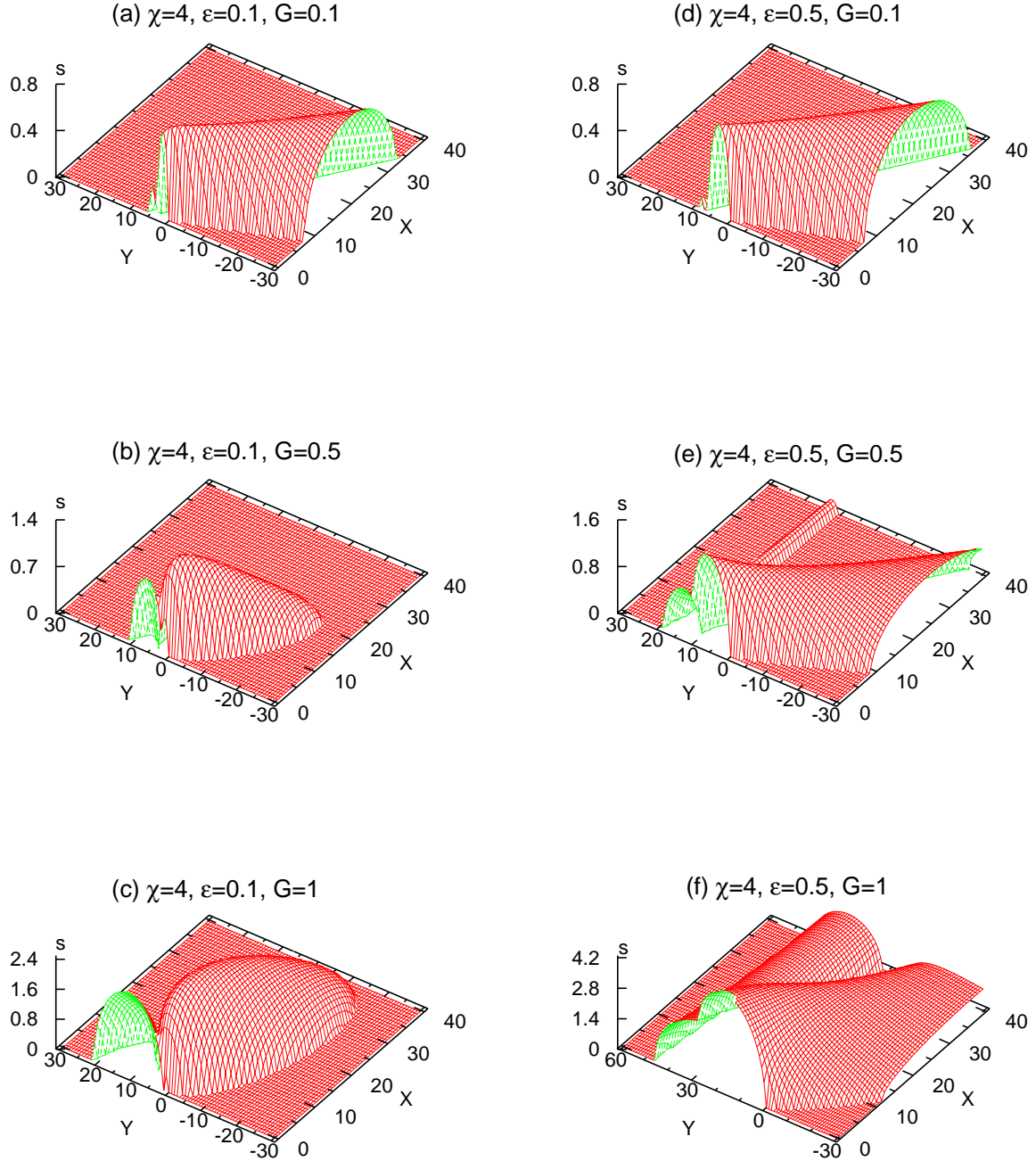


Fig. 4.— Growth rates found from Solution II for TT disks. In order to see the effect of ∇B on growth rates, we keep ε constant and change the value of G from arbitrarily chosen values of 0.1, 0.5 and 1 (see text for definitions). Left panels are for weak magnetization ($\varepsilon = 0.1$); the right panels are for strong magnetization ($\varepsilon = 0.5$). A new unstable mode comes into existence with the inclusion of ∇B . See Table 1 for maximum values of the growth rates (s_m).

3.3. Growth rates in case of $\nabla B \neq 0$ and $\nabla v_{\perp} \neq 0$

In the previous solution, we assumed that the magnetization current produces a gradient in magnetic field at the disk-magnetosphere boundary. If the magnetic moment ($\mu = mv_{\perp}^2/2B$), is conserved for drifting particles, the perpendicular velocity of the particles vary while they enter into and exit from the higher magnetic field regions. Therefore, a gradient in particles' perpendicular velocity is produced. In Solution III, we shall not omit the third term which includes ∇v_{\perp} in Eq. (6). The graphical solutions (Solution III) are presented in Fig. 5. Fig. 5a shows the results for Keplerian rotation. Therefore $T = d \ln \Omega^2/d \ln R = -3$. The inclusion of the term containing ∇v_{\perp} both increases the maximum values of the growth rates and widens the unstable regions in the X,Y plane. If we compare Fig. 4a and 5a, we see that the maximum value of the FUR increases from 0.78 (see Fig.3a) to 1.41, and also the maximum value of the SUR increases from 0.10 to 1.52 with the inclusion of the ∇v_{\perp} . In Figs 5b and 5c, we investigate the case of deviation from Keplerian rotation as a result of gradient in magnetic field and the perpendicular velocities. If the gradient in magnetic field strength and perpendicular velocity cause a change in Keplerian velocity profile of the inner disk, T should deviate from the value of “-3”. Since the values of ϵ , G and T are proportional to each other, we increase the value of ϵ and G with increasing T in Figs 5b and 5c. It is clearly seen that both the maximum values of the growth rates become higher and the regions of instability become wider with increasing ϵ , G and T (see Table 2).

4. Conclusion

We investigated the stability of a disk around CTTS by taking the diamagnetic effect into account. Plasma entry into the magnetosphere was explained by various types of plasma instabilities (e.g. the Rayleigh-Taylor instability, Kelvin-Helmholtz instability), diffusion and magnetic reconnection processes, and loss-cone mechanism in previous investigations. In this study, we investigated the perpendicular unstable mode produced by MRI which may be an alternative mechanism in guiding the plasma above the disk at the magnetospheric boundary. The main conclusions of our study can be summarized as follows:

1. MRI produces an unstable mode which can raise the plasma from the disk towards the vertical magnetic field lines. The diamagnetic effect modifies the growth rate and the wavelength range of the unstable mode. In the simplest case, when the field and velocity gradients produced by magnetization are not included, the region of instability widens in the (X,Y) plane with increasing magnetization parameter (ϵ).
2. A new unstable region comes into existence with the inclusion of the gradient in the magnetic field (G). The maximum growth rate of the unstable mode, s_m , depends more strongly on G than on ϵ . When we keep ϵ constant and change G, the maximum growth rate of the unstable mode increases with increasing values of G. On the other hand, the unstable region widens for higher values of ϵ .
3. The inclusion of the perpendicular velocity gradient in addition to the field gradient, increases the maximum growth rates and widens the regions of the instability. Moreover, the maximum value of

the growth rates increase with increasing gradient in perpendicular velocity. As a result, MRI becomes more powerful when we include the gradients in magnetic field and perpendicular velocity.

In the Hall-dominated regime electrons are frozen-into the magnetic field but ions are coupled to the neutrals. At the inner radius of the disk this situation enhances the diamagnetic current density, in turn, sharpens the magnetic field gradient. The modification to the growth rate by the magnetic field gradient may be seen in Figs. 3-5. The higher the magnitude of the gradient the greater the growth rate. In this respect, Wardle & Salmeron (2012) investigated the effect of the Hall diffusion on the stability of the Keplerian disk. They argue that in PPDs Ohm and ambipolar diffusion have a stabilizing role while the Hall effect either stabilizes or destabilizes the disk depending on the orientations of the magnetic field and the rotation axes. And they warn the reader that small dust grains may remove the electrons through recombination and the MRI-active column density reduces and MRI becomes irrelevant in PPDs.

As a result of the growing amplitude of the slow and/or standing waves produced in the disk-magnetosphere boundary of the magnetized star, we may expect that the disk fluid can be lifted towards the magnetic field lines with an approximately zero pitch angle. Zero pitch angle means that the plasma particles will seek their magnetic mirrors at the regions of higher magnetic field. It is highly probable that the particles will not be reflected until they reach the magnetic polar regions. Therefore, they will eventually hit the polar caps. The amplitude of the wave and the velocity of the disk fluid along the magnetic field lines determine the effectiveness of the lifting process. But this may be a subject of a study of non-linear regimes.

Romanova et al. (2011) stress on the fact that “the turbulence in the disk is initiated and supported by the magneto-rotational instability”. This means that MRI producing conditions, i.e., diamagnetic current etc. are continuous. Turbulence should not be considered as noise or disorder. At the macroscopic scale it may appear as chaotic but at microscopic scale turbulence reveals itself as highly organized. Drifting charged particles at the closed field lines of the magnetosphere move in a coherent way so that the diamagnetic current persists within the multiple time and length scales of turbulence. We may qualitatively argue that diamagnetic current and the magnetic field it produces may bring about a magnetic field gradient which in return triggers MRI and causes the laminar flow go turbulent. We should emphasize that in this study we work in the linear regime not in the non-linear one. So that we are not in a position to claim that the MRI will lead to turbulence at the non-linear regime.

Above all, it is yet to be seen as to whether the instability grows into turbulence. This requires a numerical simulation which will be the subject of a future study.

Our special thanks go to A. R. King and R. Lovelace for helpful suggestions and B. Kalomeni and G. James for reading the manuscript. SD appreciates the Theoretical Astrophysics Group for their hospitality. We dedicate this study to the honorable scientific and organizational effort given to the Turkish Astronomy by Prof. Dr. Zeki Aslan. This work is supported by Turkish Academy of Sciences (TÜBA) Doctoral Fellowship. This study is a part of PhD project of SD.

REFERENCES

- Alexander, R. 2008, *NewAR*, 52, 60
- Armitage, P. J. 2011, *ARA&A*, 49, 195
- Arons, J., & Lea, S. M. 1976, *ApJ*, 207, 914
- Bai, X.-N. 2011, *ApJ*, 739, 50
- Balbus, S. A., & Hawley, J. F. 1991, *ApJ*, 376, 214
- Balbus, S. A., & Hawley, J. F. 1998, *RvMP*, 70, 1
- Balbus, S. A., & Terquem, C. 2001, *ApJ*, 552, 235
- Bodo, G., Ghisellini, G., & Trussoni, E. 1992, *MNRAS*, 255, 694
- Bouvier, J., Alencar, S.H.P., Harries, T.J., Johns-Krull, C.M. & Romanova, M.M. 2006, arXiv:astro-ph/0603498v2
- Camenzind, M. 1990, *Reviews in Modern Astronomy*, 3, 234
- Devlen, E., & Pekünlü, E. R. 2007, *MNRAS*, 377, 1245
- Donati, J.-F., Gregory, S. G., Alencar, S. H. P., et al. 2011, *MNRAS*, 417, 472
- Elsner, R. F., & Lamb, F. K. 1977, *ApJ*, 215, 897
- Elsner, R. F., & Lamb, F. K. 1984, *ApJ*, 278, 326
- Fridman, A. M., Marov, M. Y., & Kovalenko, I. G. (eds.) 2006, *Astrophysical Disks; Collective and Stochastic Phenomena*, Springer, The Netherlands
- Fu, W., & Lai, D. 2012, *MNRAS*, 423, 831
- Ghosh, P., & Lamb, F. K. 1978, *ApJ*, 223, L83
- Ghosh, P., & Lamb, F. K. 1979, *ApJ*, 234, 296
- Glassgold, A. E., Najita, J. R., & Igea, J. 2007, *ApJ*, 656, 515
- Johns-Krull, C. M., & Gafford, A. D. 2002, *ApJ*, 573, 685
- Johns-Krull, C. M. 2007, *ApJ*, 664, 975
- Königl, A. 1991, *ApJL*, 370, L39
- Kulkarni, A. K., & Romanova, M. M. 2005, *ApJ*, 633, 349

- Küker, M., Henning, T., Rüdiger, G. 2003, ApJ, 589, 397
- Lamb, F. K., Pethick, C. J., & Pines, D. 1973, ApJ, 184, 271
- Li, J., Wickramasinghe, D. T., & Ruediger, G. 1996, ApJ, 469, 765
- Long, M., Romanova, M. M., & Lovelace, R. V. E. 2008, MNRAS, 386, 1274
- Lovelace, R. V. E., Romanova, M. M., & Bisnovatyi-Kogan, G. S. 1995, MNRAS, 275, 244
- Miller, K. A., & Stone, J. M. 1997, ApJ, 489, 890
- Muzerolle, J., Hartmann, L., & Calvet, N. 1998, AJ, 116, 455
- Prigogine, I., Stengers, I., & Toffler, A. 1984, Order out of chaos, Bantam, New York
- Pringle, J. E., & Rees, M. J. 1972, A&A, 21, 1
- Romanova, M. M., Ustyugova, G. V., Koldoba, A. V., & Lovelace, R. V. E. 2002, ApJ, 578, 420
- Romanova, M. M., Ustyugova, G. V., Koldoba, A. V., & Lovelace, R. V. E. 2011, MNRAS, 416, 416
- Rüdiger, G., & Shalybkov, D., 2004, PhysRevE, 69, 016303
- Singal, A. K. 1986, A&A, 155, 242
- Somov, B. V. 2006, Plasma Astrophysics, Part I: Fundamentals and Practice. By Boris V. Somov, Springer, Moscow
- Spruit, H. C., & Taam, R. E. 1993, ApJ, 402, 593
- Stempels, H. C., & Piskunov, N. 2002, A&A, 391, 595
- Strassmeier, K. G., Rice, J. B., Ritter, A., et al. 2005, A&A, 440, 1105
- Uchida, Y., & Shibata, K. 1985, PASJ, 37, 515
- Varnière, P., & Tagger, M. 2002, A&A, 394, 329
- Wardle, M. 1999, MNRAS, 307, 849
- Wardle, M., & Salmeron, R. 2012, MNRAS, 422, 2737

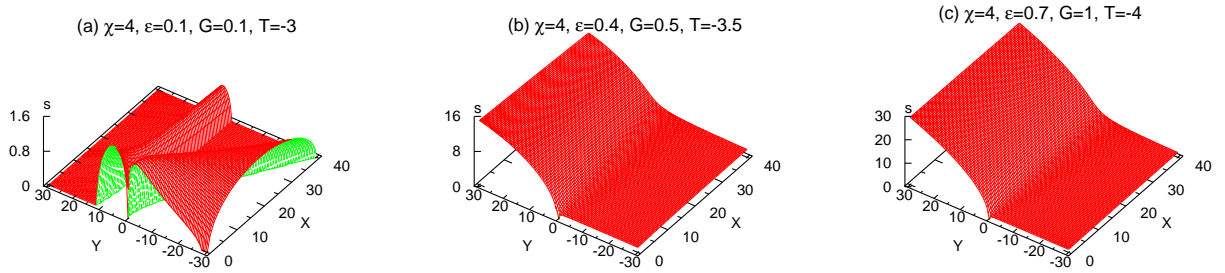


Fig. 5.— Growth rates found from Solution III. With the inclusion of ∇v_{\perp} the maximum values of the growth rates increase and the unstable regions widen in the X,Y plane. See Table 2 for maximum values of the growth rates.